CLNS 96/1441 November 1996

Experimental Tests of Lepton Universality in Tau Decay from CLEO *

Brian K. Heltsley (representing the CLEO Collaboration)

Laboratory of Nuclear Studies, Cornell University, Ithaca, NY 14853 USA

The branching fractions for $\tau \to e\nu\nu_\tau$, $\mu\nu\nu_\tau$, and $h\nu_\tau$ are measured using data collected with the CLEO detector at the CESR e^+e^- collider: $\mathcal{B}_e = 0.1776 \pm 0.0006 \pm 0.0017$, $\mathcal{B}_\mu = 0.1737 \pm 0.0008 \pm 0.0018$, and $\mathcal{B}_h = 0.1152 \pm 0.0005 \pm 0.0012$, where the first errors are statistical, the second systematic, and h refers either to a charged π or K. Also measured is the tau mass, $m_\tau = (1778.2 \pm 1.4)$ MeV. Lepton universality is affirmed by the resulting relative branching fractions ($\mathcal{B}_\mu/\mathcal{B}_e = 0.9777 \pm 0.0063 \pm 0.0087$, $\mathcal{B}_h/\mathcal{B}_e = 0.6484 \pm 0.0041 \pm 0.0060$) and the charged-current gauge coupling-constant ratios ($g_\mu/g_e = 1.0026 \pm 0.0055$, $g_\tau/g_\mu = 0.9989 \pm 0.0098$). The tau mass result may be recast as a tau neutrino mass limit, $m_{\nu_\tau} < 60$ MeV at 95% CL.

1. Introduction

The Standard Model predicts unambiguous and quite simple relationships between the tau lifetime, mass, and several of its branching fractions. Measurement of these parameters to the highest possible precision is essential; deviations from the predictions at any level could signal the presence of physics beyond our present understanding. This presentation describes determinations of the tau mass, its branching fractions to e, μ, and π/K, their relationships to the tau lifetime, and compares the results with predictions.

Lepton universality requires that the charged-current gauge coupling strengths be identical: $g_e = g_\mu = g_\tau$. μ-e universality is tested in the ratio of muonic to electronic tau decay rates as

$$\left(\frac{g_\mu}{g_e}\right)^2 = \frac{f(x_e)}{f(x_\mu)} \frac{B(\tau \to \mu\nu\nu)}{B(\tau \to e\nu\nu)} = \frac{1}{0.9726} \frac{\mathcal{B}_\mu}{\mathcal{B}_e} \quad (1)$$

where $x_\ell = (m_\ell/m_\tau)^2$, $f(x) = 1 - 8x + 8x^3 - x^4 - 12x^2 \ln x$. Comparing electronic tau decay with that of the muon probes τ-μ universality:

$$\left(\frac{g_\tau}{g_\mu}\right)^2 = \frac{\tau_\mu}{\tau_\tau}\left(\frac{m_\mu}{m_\tau}\right)^5 \frac{B(\tau \to e\nu\nu)}{B(\mu \to e\nu\nu)} \times (1+\delta_W)(1+\delta_\gamma) = 28924 \text{ fs GeV}^5 \frac{\mathcal{B}_e}{\tau_\tau\, m_\tau^5} \quad (2)$$

where $\delta_W = -2.9 \times 10^{-4}$ and $\delta_\gamma = 8.6 \times 10^{-5}$ are the weak and electromagnetic radiative corrections [1]. A second measure is obtained by comparing the muonic decays of the pion and kaon with the pionic and kaonic decays of the tau. If

$$H_h = \frac{1+\delta_h}{\tau_h\, m_h}\left(\frac{1 - m_h^2/m_\tau^2}{1 - m_\mu^2/m_h^2}\right)^2 B(h \to \mu\nu) \quad (3)$$

then

$$\left(\frac{g_\tau}{g_\mu}\right)^2 = \frac{2\, m_\mu^2}{\tau_\tau\, m_\tau^3} \frac{B(\tau \to \pi\nu) + B(\tau \to K\nu)}{H_\pi + H_K} = 14021 \text{ fs GeV}^3 \frac{\mathcal{B}_h}{\tau_\tau\, m_\tau^3} \quad (4)$$

where $\delta_\pi = 0.0016^{+0.0009}_{-0.0014}$ and $\delta_K = 0.0099^{+0.0017}_{-0.0026}$ are electromagnetic radiative corrections [2,3]. One or more of the ratios in Eqs. (1), (3), and (4) will deviate from unity in many extensions of the minimal standard model [4].

A consequence of Eqs. (2) and (4), independent of universality, is the predicted ratio

$$\frac{\mathcal{B}_h}{\mathcal{B}_e} \equiv \frac{B(\tau \to \pi\nu) + B(\tau \to K\nu)}{B(\tau \to e\nu\nu)} = \tau_\mu \frac{m_\mu^3}{m_\tau^2} \frac{H_\pi + H_K}{(1+\delta_W)(1+\delta_\gamma)} = \left(\frac{1.4366 \text{ GeV}}{m_\tau}\right)^2 \quad (5)$$

*Talk at the *Fourth International Workshop on Tau Lepton Physics*, Estes Park, Colorado, 16-19 September 1996.

Here we determine m_τ, $\mathcal{B}_e$, $\mathcal{B}_\mu$, and $\mathcal{B}_h$ using tau-pair decays produced by e^+e^- collisions near $\sqrt{s}$=10.6 GeV at the Cornell Electron Storage Ring (CESR) and measured in the CLEO detector. The branching fraction analysis uses nine tau-pair decay modes: ee, $\mu\mu$, hh, $e\mu$, eh, μh, ρe, $\rho\mu$, and ρh, where $h\equiv\pi/K$, and ρ signifies an h accompanied by at least one π^0. A "minimum kinematically allowable tau mass" is computed for each hh event, and the shape of the resulting distribution fit for m_τ.

2. Apparatus

CLEO II is a general purpose detector [6]. Three concentric drift chambers in a 1.5 T axial magnetic field provide charged particle momentum-vector determination. Surrounding the drift chambers, but inside the superconducting magnet coil, is a calorimeter of 7800 CsI(Tl) crystals with silicon photodiode readout. Muons are identified by their penetration through the calorimeter, coil, and one or more of three 36 cm-thick slabs of magnet iron; three layers of Iarocci tube chambers instrument the gap behind each slab. Fast trigger signals and particle time-of-flight (TF) are provided by scintillation counters located just inside the calorimeter. A three-tier hardware trigger system [7] takes input from the calorimeter, tracking chambers, and TF counters to form different combinations of requirements that force event readout. A fourth-level trigger implemented in software filters events based upon information assembled from the entire detector.

3. Event Selection

Selected events must have exactly two good charged particle tracks required to be of opposite charge, have momenta scaled to the beam energy $x_\pm\equiv p_\pm/E_b$ satisfying $0.1<x_\pm<0.9$, impact parameters $|d_\pm|<2$ mm, and $|\cos\theta_\pm|<0.7$, where θ is the polar angle with respect to the e^+ beam direction. Defining the acoplanarity $\xi\equiv||\phi_+-\phi_-|-\pi|$ as the two-track acollinearity in azimuth, $x_t\equiv p_t/E_b$ as the component of missing momentum transverse to the beam, scaled to the beam energy, and $|\cos\theta_{mis}|$ as the direction of this missing momentum, the two tracks must have $0.05<\xi<1.5$, $x_t>0.1$, and $|\cos\theta_{mis}|<0.8$.

Electron and muon identification criteria establish for each charged track, with some probability, its identity as an e, μ, or h. The symbol h is defined operationally as "not identified a lepton". The criteria are chosen to have high efficiencies for signal modes and small backgrounds from non-signal tau-decay modes. Electrons are identified with scaled momenta $x_\pm>0.1$; muons and hadrons with $x_\pm>0.285$. Electron criteria require that $E_\pm/p_\pm>0.85$, and that its drift chamber specific-ionization (dE/dx) be no lower than 2σ below that expected for an electron. Muon criteria demand that the track deposit $E_\pm<0.6$ GeV in the calorimeter, consistent with a minimum-ionizing particle, and that there be hits in the muon detection system matched to the track.

Radiative QED backgrounds and tau decay modes with hard π^0's are discriminated against by requiring any detected photons, excluding those in an identified ρ-tag, to have scaled energy $x_\gamma<0.10$. To exclude events in which a photon hides in a track's calorimeter shower, each track's calorimeter-energy-to-momentum ratio must satisfy $E_\pm/p_\pm<1.1$. Any photon-like shower nearest in angle to an identified lepton must satisfy $x'_\gamma<0.01$. To reduce dependence upon the simulation of hadronic interactions in the calorimeter, a different strategy is employed on the h-side of an event: the invariant mass of the h (assuming a π mass) and all photons must satisfy $M_s<0.4$ GeV.

There are additional mode-specific criteria. For high efficiency triggering on calorimeter energy in $e\mu$ and eh events, the electron scaled momentum must satisfy $x_\pm>0.235$. To suppress $e^+e^-\gamma$ and $\mu^+\mu^-\gamma$ contamination, we require $(x_++x_-)<1.5$ for the ee and $\mu\mu$ modes. Hardware trigger criteria with high and measurable efficiencies are required for each mode.

The $\ell\ell\gamma\gamma$ and $ee\ell\ell$ final states can survive the above selection criteria. To suppress these backgrounds we use the variable $\sin\Theta_{\rm min}\equiv x_t/(2-x_+-x_-)$. Energy-momentum conservation makes $\Theta_{\rm min}$ the minimum polar angle of any unseen particles. For the ee and $\mu\mu$ modes, we require $\Theta_{\rm min}>0.18$.

4. Branching Fraction Analysis

Product branching fractions for tau-pair decays to the final state ab are computed as

$$\mathcal{B}_a \times \mathcal{B}_b = \frac{n \times (1-f)}{(\mathcal{T} \times \mathcal{P} \times \mathcal{A}) \times N_{\tau\tau} \times (2-\delta_{ab})} \quad (6)$$

where n is the number of events; f is the fractional background in the sample from tau and non-tau sources; the efficiency $\mathcal{A} \times \mathcal{P} \times \mathcal{T}$ includes effects of triggering ($\mathcal{T}$), particle identification ($\mathcal{P}$), and acceptance ($\mathcal{A}$); $N_{\tau\tau}$ is the number of tau-pairs produced during data-taking; and the Kronecker-δ accounts for the case when a=b. The measured event tallies, efficiencies, backgrounds, and resulting product branching fractions are shown in Table 1.

For efficiencies and feed-across, tau-pairs were generated and decayed with the KORALB [9] program coupled to a GEANT [10] -based detector simulation, equivalent to ~3 times the data sample. Branching ratios used in this Monte Carlo (MC) are consistent with world-averages [5].

4.1. Normalization

The number of tau-pairs is computed as the product of the tau-pair cross section and the integrated luminosity, summed over all runs, $N_{\tau\tau}$=$\sum_i \{\sigma_0(s_i) \times (1+\delta_\tau)\} \times \mathcal{L}_i$, in which $\sigma_0(s_i)$ is the point cross section evaluated at the square of the center-of-mass energy s_i, the integrated luminosity $\mathcal{L}_i$ is measured [8] using wide angle Bhabha, μ-pair, and $\gamma\gamma$ final states with a relative error of 1%, and the theoretical factor adjusting the point cross section for non-zero tau mass effects and initial and final state radiative corrections [9] is $(1+\delta_\tau)$=1.1732, also with a relative error of 1%. The total integrated luminosity is 3.555 fb^{-1}, corresponding to $N_{\tau\tau}$=(3.250±0.046)×10^6. Theoretical uncertainties in radiative corrections for $\gamma\gamma$, e^+e^-, $\mu^+\mu^-$, and $\tau^+\tau^-$ final states dominate the error in $N_{\tau\tau}$.

4.2. Efficiencies

The trigger efficiency $\mathcal{T}$ for each mode separates naturally into several independent subefficiencies, which account for TF, crystal, tracking, and software trigger components. All these components are determined from the data alone.

All particle identification probabilities are measured using subsets of the data with tracks tagged as leptons or hadrons. The efficiencies $P(e\to e)\approx(97.7\pm0.15)\%$ and $P(\mu\to\mu)\approx(93.0\pm0.30)\%$, are measured with radiative lepton-pairs and two-photon events from the data. By-products of these efficiencies are the lepton-faking-hadron rates $P(\ell\to h)$=$1-P(\ell\to\ell)$. The fake rates $P(h\to e)\approx$0.1-0.5% and $P(h\to\mu)\approx$1-5%, both with relative errors of ±15%, are measured with $\tau\to h\pi^0\nu$ decays. The hadron identification probability is $P(h\to h)$= $1-P(h\to e)\ -P(h\to\mu)\approx(97.7\pm0.3)\%$.

To determine the net two-particle identification efficiency for a given tau-pair decay mode, for each MC signal event we find the identification probabilities for both tracks, as tabulated by particle species, momentum, polar angle, and charge. The product of these probabilities is then averaged over all generated signal events.

The acceptance is determined from MC by dividing the number of signal events satisfying all the selection criteria by the total number generated. The total error assigned to the acceptance for each mode is the quadrature sum of the statistical error from MC and an additional 1.0% relative error to account for possible systematic effects of the detector simulation or event generator. The latter error is assumed to consist of equal parts (in quadrature) mode-specific (0.7%) and mode-common (0.7%) errors.

4.3. Backgrounds

Table 2 shows the estimated background fractions. Feed-across is the dominant background in all modes, and is computed from MC using the particle identification weights measured in the data, applying signal trigger efficiencies, and normalizing to luminosity. The uncertainties are dominated by the errors on particle identification but also include contributions from trigger efficiency, luminosity, and branching fractions. Modes with K^0_L's are considered background and are explicitly subtracted.

All other backgrounds are small. Tails of the observed track impact parameter distributions yield estimates of the cosmic ray level. Remaining sources rely upon MC simulations of *eeee*, [11]

Table 1
Product Branching Fraction Components

ab	n	$\mathcal{A}(\%)$	$\mathcal{P}(\%)$	$\mathcal{T}(\%)$	$f(\%)$	$\mathcal{B}_a \times \mathcal{B}_b$ (%)
ee	11019	11.304±0.123	95.59±0.30	97.51±0.52	1.62±0.48	3.166±0.030±0.062
$\mu\mu$	3846	5.443±0.060	86.01±0.57	79.00±1.23	4.10±0.63	3.069±0.049±0.078
hh	4970	9.900±0.129	95.29±0.65	86.20±0.93	27.68±0.87	1.360±0.019±0.035
$e\mu$	17364	9.706±0.104	90.75±0.33	96.29±0.63	2.38±0.38	3.075±0.023±0.060
eh	14880	10.102±0.109	95.45±0.36	97.03±0.66	17.43±0.68	2.021±0.017±0.043
μh	9739	7.868±0.090	90.62±0.43	83.60±1.00	20.01±1.12	2.011±0.020±0.053
ρe	15314	3.909±0.043	96.42±0.25	97.35±0.63	1.68±0.12	6.313±0.051±0.122
$\rho\mu$	11505	3.148±0.035	91.69±0.35	97.44±0.66	3.09±0.28	6.099±0.057±0.121
ρh	9846	3.259±0.038	96.34±0.46	97.51±0.71	18.28±0.52	4.043±0.041±0.086

Table 2
Background Fractions (%). Unlisted errors are 100% of the background estimate. Here $\ell \equiv e/\mu$.

ab	$\tau^+\tau^-$	Cosmic	$ee\tau\tau$	$\ell\ell$	$ee\ell\ell$
ee	0.83±0.13	–	0.24	0.32	0.23
$\mu\mu$	3.62±0.58	0.15±0.07	0.11	0.22	–
hh	27.16±0.81	0.10±0.05	0.29	0.06	0.07
$e\mu$	2.13±0.34	–	0.12	–	0.13
eh	16.78±0.50	–	0.32	–	0.33
μh	18.51±0.56	0.13±0.07	0.12	0.34	0.90
ρe	1.57±0.06	–	0.10	–	0.01
$\rho\mu$	3.09±0.28	–	–	–	–
ρh	18.08±0.49	0.01±0.01	0.16	–	0.03

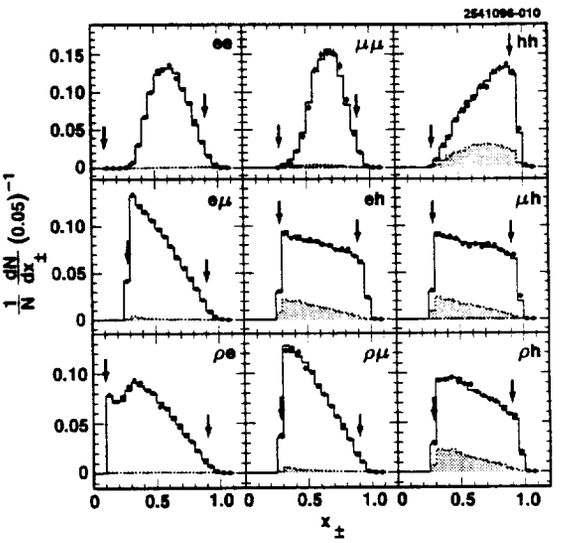

Figure 1. Distributions in $x_\pm$; the higher momentum track is plotted for ee, $\mu\mu$, and hh, the muon's for $e\mu$, the hadron's for eh and μh, and the track's opposite the ρ for the ρ-tag modes.

$ee\mu\mu$, [12] $ee\tau\tau$, [12] ee, [13,14] and $\mu\mu$ [15] final states. Backgrounds from $e^+e^- \to q\bar{q} \to$hadrons and $e^+e^- \to \Upsilon(4S) \to B\bar{B}$ are negligible.

The cross sections for these QED processes are quite large compared to those probed in this analysis. The selection criteria must suppress them by factors up to 10^6 to attain sub-1% contaminations. At this level, it is difficult to verify accurate normalization of these processes, their radiative corrections, and simulated detector response. Hence the MC predictions for these final states are each normalized to the data in a region outside of, but adjacent to, the nominal allowed region for a given mode. The resulting scale factors are 2.9 for Bhabhas, 1.6 for μ-pairs, 0.77 for $eeee$, and 0.57 for $ee\mu\mu$. Relative errors of ±100% allow for the *ad hoc* nature of this procedure.

4.4. Systematic Checks

Distributions in variables relevant to the selection process are modeled well by the MC, some examples of which are shown in Figs. 1-4. The data (solid circles) and MC (histograms) are normalized to unit area inside the nominal cuts. The lightly shaded regions correspond to tau-pair feed-across, and the vertical arrows to cut values. Variations of the product branching frac-

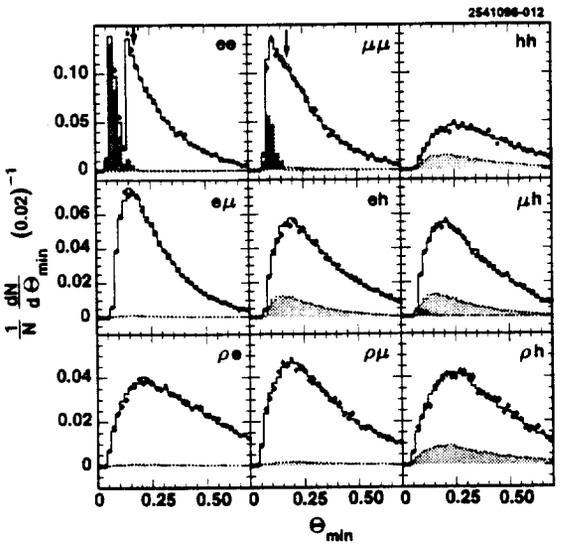

Figure 2. Distributions in $\Theta_{\rm min}$. The darkly shaded regions in the ee and $\mu\mu$ plots at small $\Theta_{\rm min}$ indicate the MC predictions for $eeee$ and $ee\mu\mu$ backgrounds, respectively. The first 7 bins in the ee plot are scaled down by a factor of 8.

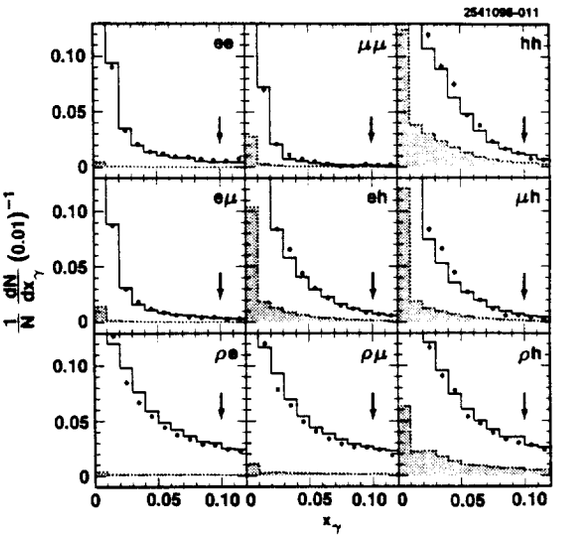

Figure 3. Distributions in x_γ.

tions with reasonably altered cuts are consistent with those expected from the assigned statistical and systematic errors. The product branching fractions are stable when divided into eleven consecutive samples of comparable size, or into on-$\Upsilon(4S)$ and below-$\Upsilon(4S)$ datasets.

4.5. Results

The measured product branching fractions can be combined to yield the desired absolute and relative tau branching fractions. For each of $\mathcal{B}_e$, $\mathcal{B}_\mu$, $\mathcal{B}_h$, $\mathcal{B}_\mu/\mathcal{B}_e$, and $\mathcal{B}_h/\mathcal{B}_e$, there are six such combinations that are independent. Five separate χ^2-fits, or weighted averages, of six methods are performed, properly accounting for the many error correlations. As an example, the fit for $\mathcal{B}_h$ is detailed in Table 3. The results are $\mathcal{B}_e$=(17.76±0.06 ±0.17)%, $\mathcal{B}_\mu$=(17.37±0.08±0.18)%, $\mathcal{B}_h$=(11.52 ±0.05±0.12)%, $\mathcal{B}_\mu/\mathcal{B}_e$=(97.77±0.63±0.87)%, and $\mathcal{B}_h/\mathcal{B}_e$=(64.84±0.41±0.60)%. The fit χ^2's are reasonable (~2.8/5 dof). Each of the five quantities is measured with a total relative error of ~1%. Sources of uncertainty are summarized in Table 4. Systematic errors dominate the $\mathcal{B}_e$, $\mathcal{B}_\mu$, $\mathcal{B}_h$ uncertainties, largely due to the error in the normalization $N_{\tau\tau}$. Statistical errors matter more for $\mathcal{B}_\mu/\mathcal{B}_e$ and $\mathcal{B}_h/\mathcal{B}_e$, for which the normalization cancels and hence plays no role.

Table 3
Fit Results for $\mathcal{B}_h$

Method	$\mathcal{B}_h$(%)	Wt
$\sqrt{\mathcal{B}_h\mathcal{B}_h}$	11.66±0.08±0.15	0.42
$\sqrt{\mathcal{B}_e\mathcal{B}_h\cdot\mathcal{B}_\rho\mathcal{B}_h/\mathcal{B}_\rho\mathcal{B}_e}$	11.38±0.09±0.15	0.29
$\sqrt{\mathcal{B}_\mu\mathcal{B}_h\cdot\mathcal{B}_\rho\mathcal{B}_h/\mathcal{B}_\rho\mathcal{B}_\mu}$	11.55±0.10±0.18	0.12
$\mathcal{B}_e\mathcal{B}_h/\sqrt{\mathcal{B}_e\mathcal{B}_e}$	11.36±0.11±0.19	0.11
$\sqrt{\mathcal{B}_e\mathcal{B}_h\cdot\mathcal{B}_\mu\mathcal{B}_h/\mathcal{B}_e\mathcal{B}_\mu}$	11.50±0.09±0.18	0.04
$\mathcal{B}_\mu\mathcal{B}_h/\sqrt{\mathcal{B}_\mu\mathcal{B}_\mu}$	11.48±0.15±0.26	0.02
Fit: χ^2=2.8/5 dof	11.52±0.05±0.12	-

An alternate method of extracting the results is to perform a simultaneous global χ^2-fit for all the branching fractions, again accounting for correla-

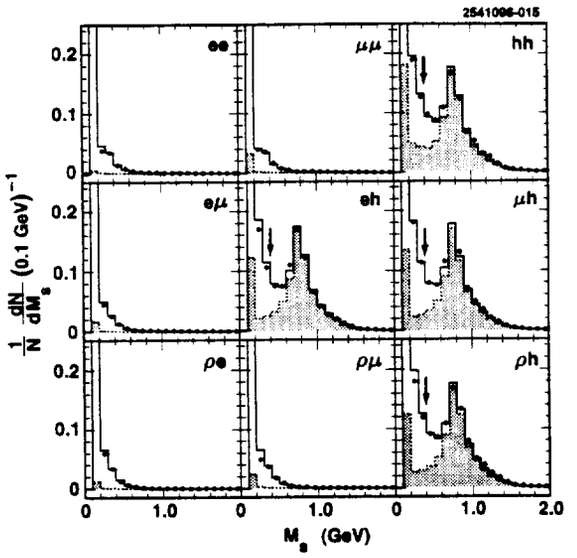

Figure 4. Distributions in M_s for one side of the event; the higher momentum track side's mass is plotted for ee, $\mu\mu$, and hh, the muon's for $e\mu$, the hadron's for eh and μh, and the track's opposite the ρ for the ρ-tag modes.

tions. The global fit gives nearly identical results (within ~0.1%, relative) and errors (within ~5%, relative) as the weighted-average technique, and yields χ^2=2.9 for five degrees of freedom.

5. Tau Mass

The most precise measurement of the tau mass comes from e^+e^- data taken at tau-pair threshold by BES, m_τ^{BES}=(1776.96$^{+0.18+0.25}_{-0.21-0.17}$) MeV [16]. The published CLEO result [17] selected $h\rho$ and $\rho\rho$ events, and by fitting the distribution of a minimum kinematically allowable tau mass $(m_\tau)_{min}$ for each event, obtaining m_τ=(1777.8±0.7±1.7) MeV. The largest contribution to the systematic error was attributable to uncertainty in π^0 energy as measured in the electromagnetic calorimeter.

Here we again employ the $(m_\tau)_{min}$-fitting technique but apply it to hh events. In comparison to our $h\rho$, $\rho\rho$ analysis, this strategy retains sensitivity to m_τ, provides a statistically independent sample, and eliminates dependence upon calorimeter calibration because no π^0 reconstruction is necessary. The tradeoffs are that the branching fractions are smaller, more emphasis is placed upon accurate momentum determinations, and special attention must be paid to eliminating QED backgrounds. This analysis is described in more detail in ref. [18].

Table 4
Relative Errors (%) by Source

Source	$\mathcal{B}_e$	$\mathcal{B}_\mu$	$\mathcal{B}_h$	$\mathcal{B}_\mu/\mathcal{B}_e$	$\mathcal{B}_h/\mathcal{B}_e$
n	0.36	0.47	0.46	0.65	0.63
$N_{\tau\tau}$	0.71	0.71	0.71	-	-
$\mathcal{A}$	0.48	0.54	0.54	0.56	0.56
$\mathcal{T}$	0.28	0.40	0.37	0.51	0.48
f	0.19	0.23	0.39	0.32	0.43
$\mathcal{P}$	0.16	0.32	0.31	0.36	0.34
Sum	1.00	1.15	1.18	1.10	1.12

Energy-momentum conservation allows each hadronic daughter's momentum vector to determine a cone on which the parent τ direction lies, assuming no initial or final state radiation and a single massless unobserved neutrino in each decay. The opening angle of these two cones depends on the value of the parent mass, m_τ. Reflecting one of the two cones through the origin then gives two cones that intersect, in general on more than one ray. The parent mass can be varied until the cones have only one common line of intersection; this then is $(m_\tau)_{min}$, the smallest kinematically allowed value of the parent mass for that event. Measurement errors, initial state radiation, and non-tau backgrounds can yield events with $(m_\tau)_{min}>m_\tau$, but proper selection criteria can minimize these sources, thereby maintaining a sharp dropoff, or "edge", in the $(m_\tau)_{min}$ distribution near the true value of m_τ.

Unlike our $h\rho$, $\rho\rho$ analysis, a closed-form few-term function is not used to fit the data or MC. Instead, the actual shape of the simulation distribution is used, after fitting it with a cubic spline with eight knots so as to avoid binning effects. This spline shape is then used with floating normalization to fit the data's distribution

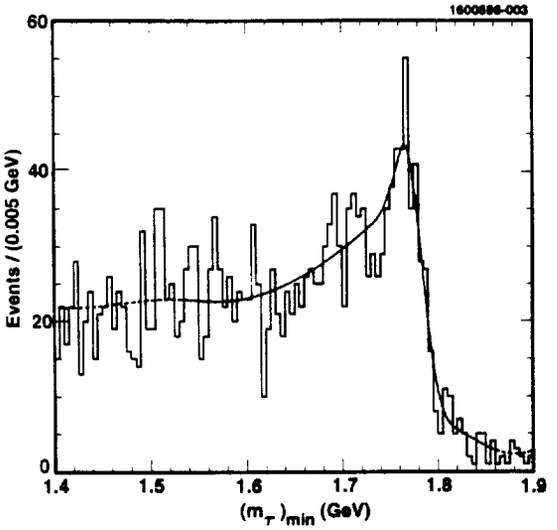

Figure 5. $(m_\tau)_{min}$ distribution from data (histogram) and spline fit (curve).

of $(m_\tau)_{min}$, with the only other free parameter being the shift relative to the MC tau mass (1777 MeV). The fit of the spline to the data distribution for $(m_\tau)_{min}$ is shown in Fig. 5. Systematic errors (in MeV) include those attributed to simulation statistics (0.8), non-tau backgrounds and feed-across (0.7), momentum scale (0.4), fit linearity (0.3), momentum resolution (0.2), radiative corrections (0.2), and beam energy uncertainty (0.1).

The result is m_τ=(1778.7±1.6±1.2) MeV for the hh analysis. It can be combined with that of our published $h\rho$, $\rho\rho$ analysis, with which it is consistent. When common and independent errors are treated properly, the two results receive comparable weight and give a combined measurement of m_τ=(1778.2±1.4) MeV.

The algebraic equation employed in this analysis for extracting m_τ involves the mass of the tau neutrino, m_{ν_τ}, which has heretofore been assumed to be zero. The fitted tau mass from this analysis can be expressed in terms of the neutrino mass and the true tau mass, for which we take m_τ^{BES} because it has no dependence on m_{ν_τ}, as $m_\tau^{FIT} \simeq m_\tau^{BES} - (m_{\nu_\tau}^2/m_0)$ where m_0 is a mass parameter which adjusts the equation for several approximations. Using both the data and simulations, m_0 has been determined to be (1.6±0.3) GeV. We then obtain $m_{\nu_\tau}^2 = (-1.9 \pm 2.4) \times 10^3$ MeV^2. Taking the Bayesian approach [5] to limit the result to physical masses ($m_{\nu_\tau}^2 \geq 0$) yields $m_{\nu_\tau} < 60$ MeV at 95% C.L.

6. Conclusions

The CLEO branching fractions, tau mass, and tau lifetime τ_τ=289 ± 2.8 ± 4.0 fs [23] measurements can be inserted into Eqs. (1), (2), and (4), yielding, respectively, the ratios of coupling constants

$$\frac{g_\mu}{g_e} = 1.0026 \pm 0.0055 \quad (\text{using } \mathcal{B}_\mu/\mathcal{B}_e) \qquad (7)$$

$$\frac{g_\tau}{g_\mu} = 0.9999 \pm 0.0100 \quad (\text{using } \mathcal{B}_e,\ \tau_\tau,\ m_\tau) \qquad (8)$$

$$\frac{g_\tau}{g_\mu} = 0.9970 \pm 0.0103 \quad (\text{using } \mathcal{B}_h,\ \tau_\tau,\ m_\tau) \qquad (9)$$

each of which is consistent with unity, and hence with lepton universality. The μ-e universality ratio in Eq. (7), which relates to transverse-W coupling, is about a factor of three less precise than that obtained from leptonic pion decay [21,22], which, however, applies only to longitudinal-W coupling [2–4]. The lifetime uncertainty dominates the error in both τ-μ universality measurements; they are almost completely correlated due to their similar dependence upon τ_τ, $N_{\tau\tau}$, and m_τ. Combining them yields g_τ/g_μ=0.9989±0.0098. If instead the world-average lifetime τ_τ=(291.0±1.5) fs [5] and mass m_τ=1777.00$^{+0.30}_{-0.27}$ [5] are used, we obtain g_τ/g_μ=0.9981±0.0056 using $\mathcal{B}_e$ and g_τ/g_μ=0.9946±0.0064 using $\mathcal{B}_h$, or, combining them, g_τ/g_μ=0.9969±0.0053. Here the branching fraction uncertainties dominate the errors.

The branching fractions and coupling-constant ratios measured here are consistent with and compare favorably in precision to other measurements [5]. In particular, the $\mathcal{B}_h$ and $\mathcal{B}_h/\mathcal{B}_e$ values presented here are the most precise published measurements, and are consistent with the prediction

of Eq. (5), which is $\mathcal{B}_h/\mathcal{B}_e$=0.6527±0.0010 when the CLEO value of m_τ is used.

In summary, we have measured absolute branching fractions for $\tau\to e\nu\nu_\tau$, $\tau\to\mu\nu\nu_\tau$, $\tau\to h\nu_\tau$, and their ratios to one another, with relative errors of 1%. The tau mass has been measured with a relative error of 0.08%. The results show no indication for deviations from the Standard Model predictions. CLEO is the only single experiment to have measured the tau lifetime, mass, and $e/\mu/h$ branching fractions simultaneously, providing all the ingredients for lepton universality tests in tau decay: μ-e and τ-μ universality are verified at the 0.5% and 1% levels, respectively.

7. Acknowledgments

I am indebted to my CLEO colleagues for making this analysis possible, and gratefully acknowledge the effort of the CESR staff in providing excellent luminosity and running conditions. This work was supported by the National Science Foundation, the U.S. Department of Energy, the Heisenberg Foundation, the Alexander von Humboldt Stiftung, Research Corporation, the Natural Sciences and Engineering Research Council of Canada, and the A.P. Sloan Foundation.

REFERENCES

1. W.J. Marciano and A. Sirlin, Phys. Rev. Lett. **61**, 1815 (1988).
2. R. Decker and M. Finkemeier, Phys. Lett. B **334**, 199 (1994) and Nucl. Phys. **B438**, 17 (1995).
3. W.J. Marciano and A. Sirlin, Phys. Rev. Lett. **71**, 3629 (1993).
4. W.J. Marciano, *Proceedings of the Third Workshop on Tau Lepton Physics*, edited by L. Rolandi, North-Holland, Nucl. Phys. B (Proc. Suppl.) **40**, 3 (1995).
5. Particle Data Group, R.M. Barnett *et al.*, Phys. Rev. D **54**, 1 (1996).
6. CLEO Collaboration, Y. Kubota *et al.*, Nucl. Instrum. Methods A **320**, 66 (1992).
7. C. Bebek *et al.*, Nucl. Instr. Methods A **302**, 261 (1991).
8. CLEO Collaboration, G. Crawford *et al.*, Nucl. Instrum. Methods A **345**, 429 (1994).
9. KORALB (v.2.2) / TAUOLA (v.2.4): S. Jadach and Z. Was, Comput. Phys. Commun. **36**, 191 (1985); **64**, 267 (1991); S. Jadach, J.H. Kühn, and Z. Was, *ibid.* **64**, 275 (1991); **70**, 69 (1992), **76**, 361 (1993).
10. R. Brun *et al.*, GEANT v. 3.14, CERN DD/EE/84-1. Version 3.15 is used here.
11. J. Vermasseren, Nucl. Phys. **B229**, 347 (1983).
12. V.M. Budnev *et al.*, Phys. Rep. **15**, 181 (1975).
13. F. Berends and R. Kleiss, Nucl. Phys. **B228**, 537 (1983).
14. BHLUMI v. 1.22: S. Jadach, E. Richter-Was, B.F.L. Ward, and Z. Was, CERN-TH-6230-91 (Sept. 1991); Phys. Lett. B **268**, 253 (1991); **260**, 438 (1991); **253**, 469 (1991); S. Jadach and B.F.L. Ward, Phys. Rev. D **40**, 3582 (1989).
15. R. Kleiss and S. van der Marck, Nucl. Phys. **B342**, 61 (1990).
16. BES Collaboration, J.Z. Bai *et al.*, Phys. Rev. D **53**, 20 (1996).
17. CLEO Collaboration, R. Balest *et al.*, Phys. Rev. D **47**, R3671 (1993).
18. J. Mevissen, Cornell University Ph.D. Thesis, May 1996 (unpublished).
19. D. Acosta, Univ. of California at San Diego Ph.D. Thesis, May 1993 (unpublished).
20. CLEO Collaboration, J. Dominick *et al.*, Phys. Rev. D **50**, 3027 (1994).
21. D. Britton *et al.*, Phys. Rev. Lett. **68**, 3000 (1992).
22. C. Czapek *et al.*, Phys. Rev. Lett. **70**, 17 (1993).
23. CLEO Collaboration, R. Balest *et al.*, CLNS 96/1417, June 1996 (to be published in Phys. Lett. B).